

Next-to-leading-order QCD corrections to a vector bottomonium radiative decay into a charmonium

Yu-Dong Zhang,^a Feng Feng,^{b,c} Wen-Long Sang,^a Hong-Fei Zhang^d

^a*School of Physical Science and Technology, Southwest University, Chongqing 400700, China*

^b*China University of Mining and Technology, Beijing 100083, China*

^c*Institute of High Energy Physics and Theoretical Physics Center for Science Facilities, Chinese Academy of Sciences, Beijing 100049, China*

^d*College of Big Data Statistics, Guizhou University of Finance and Economics, Guiyang, 550025, China*

E-mail: zhangyudong@email.swu.edu.cn, F.Feng@outlook.com,
wlsang@swu.edu.cn:corresponding author, shckm2686@163.com

ABSTRACT: Within the framework of nonrelativistic QCD (NRQCD) factorization, we calculate the next-to-leading-order (NLO) perturbative corrections to the radiative decay $\Upsilon \rightarrow \eta_c(\chi_{cJ}) + \gamma$. Both the helicity amplitudes and the helicity decay widths are obtained. It is the first computation for the processes involving both bottomonium and charmonium at two-loop accuracy. By employing the Cheng-Wu theorem, we are able to convert most of complex-valued master integrals (MIs) into real-valued MIs, which makes the numerical integration much efficient. Our results indicate the $\mathcal{O}(\alpha_s)$ corrections are moderate for η_c and χ_{c2} production, and are quite marginal for χ_{c0} and χ_{c1} production. It is impressive to note the NLO corrections considerably reduce the renormalization scale dependence in both the decay widths and the branching fractions for χ_{cJ} , and slightly improve that for η_c . With the NRQCD matrix elements evaluated via the Buchmüller-Tye potential model, we find the decay width for η_c production is one-order-of-magnitude larger than χ_{cJ} production, which may provide a good opportunity to search for $\Upsilon \rightarrow \eta_c + \gamma$ in experiment. In addition, the decay width for χ_{c1} production is several times larger than those for $\chi_{c0,2}$. Finally, we find the NLO NRQCD prediction for the branching fraction of $\Upsilon \rightarrow \chi_{c1} + \gamma$ is only half of the lower bound of the experimental data measured recently by Belle. Moreover, there exists serious contradiction between theory and experiment for $\Upsilon \rightarrow \eta_c + \gamma$. The discrepancies between theory and experiment deserve further research efforts.

KEYWORDS: Quarkonium, NRQCD factorization, Radiative corrections

Contents

1	Introduction	1
2	The general formulas	2
3	NRQCD formalism for $\Upsilon \rightarrow H + \gamma$	3
4	Technical strategy of calculating SDCS	6
5	Two schemes to deal with the QED contribution	8
6	Main results	9
7	Phenomenology and discussion	11
8	Summary	16
A	Construction of various helicity projectors	16
B	Applying the Cheng-Wu theorem to deal with loop integrals	18

1 Introduction

Heavy quarkonium, composed of a pair of heavy quark and heavy antiquark, is the co-existence of several distinct mass scales, which renders it a clean platform to probe the interplay between perturbative and nonperturbative dynamics. The process of a bottomonium radiative decay into a charmonium involves two flavors of heavy quark, which may enrich our knowledge on quarkonium structure and the nonperturbative properties of QCD.

Many efforts have been devoted to searching for the hint of the process in experiment. The search for charmonium and charmonium-like states through Υ radiative decay has been performed by Belle collaboration [1–3]. Recently, the first observation of the radiative decay of the Υ into a P -wave charmonium has been reported with 6.3 standard deviations by Belle collaboration [4]: $\text{Br}(\Upsilon \rightarrow \chi_{c1} + \gamma) = 4.7_{-1.8}^{+2.4}(\text{stat})_{-0.5}^{+0.4}(\text{sys}) \times 10^{-5}$.

On the theory side, it is believed that a bottomonium radiative decay into a charmonium can be systematically described by the nonrelativistic QCD (NRQCD) factorization approach [5], which is based on the effective-field-theory formalism and directly linked with the first principles of QCD. Based on this well-established framework, the production rates of η_c and χ_{cJ} with $J = 0, 1, 2$ in the Υ radiative decays have been calculated at leading order (LO) in the strong coupling constant α_s in Ref. [6]. Very recently, the processes have been restudied by the authors in Ref. [7], where the analytical expressions were presented

in terms of the one-loop scalar Passarino-Veltman integrals. Similarly, the radiative decays of η_b or χ_{bJ} into J/ψ have also been computed in Refs. [6, 8].

It is quite disquieting that the theoretical prediction on the cross section of $\Upsilon \rightarrow \chi_{c1} + \gamma$ is much smaller than the experimental data [4]. Even worse, the LO theoretical prediction bears a strong renormalization scale dependence.

Recently, there have been great advances in the calculation of high-order radiative corrections to quarkonium inclusive and exclusive production and decay [9–24]. For many processes, the two-loop radiative corrections are significant relative to the LO results, which may substantially change the theoretical predictions [9–14, 18]. In contrast, the next-to-next-to-leading-order (NNLO) corrections to the cross sections of $J/\psi + \eta_c$ and $\eta_c(\chi_{cJ}) + \gamma$ production at B factory are moderate [20–22]. More importantly, by incorporating the NNLO corrections, the NRQCD theoretical predictions for $e^+e^- \rightarrow J/\psi + \eta_c$ and $e^+e^- \rightarrow \chi_{c1} + \gamma$ can be consistent with the experimental measurements. Encouraged by the success of the NRQCD predictions on these two processes, we compute the next-to-leading-order (NLO) corrections for $\Upsilon \rightarrow \eta_c(\chi_{cJ}) + \gamma$ in this work. For the process of a vector bottomonium radiative decay into a charmonium, the bottomonium can decay through either a photon or two gluons associated with a photon, which are called the QED process and the QCD process respectively. Since the Feynman diagrams for the QCD process start at one loop, we need to compute the two-loop corrections. For the QED process, we only need to include the one-loop corrections.

The remainder of this paper is organized as follows. In section 2, we present the general formulas for the helicity amplitudes and partial widths of $\Upsilon \rightarrow \eta_c(\chi_{cJ}) + \gamma$. In section 3, after outlining the NRQCD factorization formula, we describe the theoretical strategy to derive the NRQCD short-distance coefficients (SDCs). In section 4, we describe the technicalities encountered in the calculation. To reduce the theoretical uncertainty, we introduce two schemes to compute the QED process in section 5. Our main numerical results for the SDCs of various helicity amplitudes are presented in section 6. Section 7 is devoted to the phenomenological analysis and discussion. Finally, we summarize in section 8. In Appendix A, we present the explicit expressions of various helicity projectors introduced in section 3. In Appendix B, we describe the approach of dealing with loop integrals by Cheng-Wu theorem.

2 The general formulas

It is of some advantage to utilize the helicity amplitude formalism to analyze the hard exclusive decay process. In general, we can express the helicity partial width of $\Upsilon \rightarrow H + \gamma$ (H can be η_c or χ_{cJ}) as

$$\Gamma(\Upsilon \rightarrow H(\lambda_1) + \gamma(\lambda_2)) = \frac{1}{3} \frac{1}{2m_\Upsilon} \frac{1}{8\pi} \frac{2|\mathbf{P}|}{m_\Upsilon} |A_{\lambda_1, \lambda_2}^{(H)}|^2, \quad (2.1)$$

where m_Υ represents the mass of Υ meson and P denotes the momentum of the charmonium H . The magnitude of the three momentum of P is determined by

$$|\mathbf{P}| = \frac{\lambda^{1/2}(m_\Upsilon^2, m_H^2, 0)}{2m_\Upsilon} = \frac{m_\Upsilon^2 - m_H^2}{2m_\Upsilon}, \quad (2.2)$$

where the Källén function is defined via $\lambda(x, y, z) = x^2 + y^2 + z^2 - 2xy - 2xz - 2yz$. The spin average for the initial meson has been done, and the integration over the two-body phase space is explicitly carried out.

In eq. (2.1), λ_1 and λ_2 signify the helicities of the charmonia H and the outgoing photon. According to the angular momentum conservation, we can enumerate all the helicity amplitudes $A_{0,\pm 1}^{(\eta_c)}$, $A_{0,\pm 1}^{(\chi_{c0})}$, $A_{\pm 1,\pm 1}^{(\chi_{c1})}$, $A_{0,\pm 1}^{(\chi_{c1})}$, $A_{\pm 2,\pm 1}^{(\chi_{c2})}$, $A_{\pm 1,\pm 1}^{(\chi_{c2})}$ and $A_{0,\pm 1}^{(\chi_{c2})}$, which, however, are not independent. We can reduce the number of the helicity amplitudes by applying the relations of the parity invariance [25] $A_{\lambda_1, \lambda_2}^{(\eta_c)} = -A_{-\lambda_1, -\lambda_2}^{(\eta_c)}$, and $A_{\lambda_1, \lambda_2}^{(\chi_{cJ})} = (-1)^J A_{-\lambda_1, -\lambda_2}^{(\chi_{cJ})}$. Explicitly, we have

$$A_{0,1}^{(\eta_c)} = -A_{0,-1}^{(\eta_c)}, \quad (2.3a)$$

$$A_{0,1}^{(\chi_{c0})} = A_{0,-1}^{(\chi_{c0})}, \quad (2.3b)$$

$$A_{0,1}^{(\chi_{c1})} = -A_{0,-1}^{(\chi_{c1})}, \quad A_{1,1}^{(\chi_{c1})} = -A_{-1,-1}^{(\chi_{c1})}, \quad (2.3c)$$

$$A_{0,1}^{(\chi_{c2})} = A_{0,-1}^{(\chi_{c2})}, \quad A_{1,1}^{(\chi_{c2})} = A_{-1,-1}^{(\chi_{c2})}, \quad A_{2,1}^{(\chi_{c2})} = A_{-2,-1}^{(\chi_{c2})}. \quad (2.3d)$$

In the limit of $m_b \gg m_c$, the helicity amplitudes in (2.3) satisfy the asymptotic behavior

$$A_{\lambda_1, \lambda_2}^{(H)} \propto r^{1+|\lambda_1|}, \quad (2.4)$$

where r is defined via $r = m_c/m_b$. One power of r in eq. (2.4) originates from the large momentum transfer which is required for the heavy-quark pair to form the heavy quarkonium with small relative momentum and the other powers arise from the helicity selection rule in perturbative QCD [26, 27].

In terms of the independent helicity amplitudes, the total partial widths can be expressed as

$$\Gamma(\Upsilon \rightarrow \eta_c + \gamma) = \frac{1}{3} \frac{1}{2m_\Upsilon} \frac{1}{8\pi} \frac{2|\mathbf{P}|}{m_\Upsilon} 2 \times |A_{0,1}^{(\eta_c)}|^2, \quad (2.5a)$$

$$\Gamma(\Upsilon \rightarrow \chi_{c0} + \gamma) = \frac{1}{3} \frac{1}{2m_\Upsilon} \frac{1}{8\pi} \frac{2|\mathbf{P}|}{m_\Upsilon} 2 \times |A_{0,1}^{(\chi_{c0})}|^2, \quad (2.5b)$$

$$\Gamma(\Upsilon \rightarrow \chi_{c1} + \gamma) = \frac{1}{3} \frac{1}{2m_\Upsilon} \frac{1}{8\pi} \frac{2|\mathbf{P}|}{m_\Upsilon} 2 \times \left(|A_{0,1}^{(\chi_{c1})}|^2 + |A_{1,1}^{(\chi_{c1})}|^2 \right), \quad (2.5c)$$

$$\Gamma(\Upsilon \rightarrow \chi_{c2} + \gamma) = \frac{1}{3} \frac{1}{2m_\Upsilon} \frac{1}{8\pi} \frac{2|\mathbf{P}|}{m_\Upsilon} 2 \times \left(|A_{0,1}^{(\chi_{c2})}|^2 + |A_{1,1}^{(\chi_{c2})}|^2 + |A_{2,1}^{(\chi_{c2})}|^2 \right). \quad (2.5d)$$

3 NRQCD formalism for $\Upsilon \rightarrow H + \gamma$

According to the NRQCD formalism [5], we can factorize the helicity amplitude into

$$A_{\lambda_1, \lambda_2}^{(H)} = \sqrt{2m_\Upsilon} \sqrt{2m_H} c_{\lambda_1, \lambda_2}(H) \frac{\sqrt{\langle \mathcal{O}_\Upsilon \rangle_\Upsilon}}{m_b^{3/2}} \frac{\sqrt{\langle \mathcal{O}_H \rangle_H}}{m_c^n}, \quad (3.1)$$

where $n = \frac{3}{2}$ for η_c and $n = \frac{5}{2}$ for χ_{cJ} , $c_{\lambda_1, \lambda_2}(H)$ signifies the dimensionless SDC of the corresponding helicity amplitude, and the NRQCD long-distance matrix elements (LDMEs)

are defined via $\langle \mathcal{O}_h \rangle_h \equiv \langle h | \psi^\dagger \mathcal{K}_h \chi \chi^\dagger \mathcal{K}_h \psi | h \rangle$ with

$$\mathcal{K}_\Upsilon = \boldsymbol{\sigma}, \quad (3.2a)$$

$$\mathcal{K}_{\chi_{c0}} = \frac{1}{\sqrt{3}} \left(-\frac{i}{2} \overleftrightarrow{\mathbf{D}} \cdot \boldsymbol{\sigma} \right), \quad (3.2b)$$

$$\mathcal{K}_{\chi_{c1}} = \frac{1}{\sqrt{2}} \left(-\frac{i}{2} \overleftrightarrow{\mathbf{D}} \times \boldsymbol{\sigma} \right), \quad (3.2c)$$

$$\mathcal{K}_{\chi_{c2}} = -\frac{i}{2} \overleftrightarrow{D}^{(i} \sigma^{j)}. \quad (3.2d)$$

In $\langle \mathcal{O}_h \rangle_h$, ψ and χ are the Pauli spinor fields annihilating a heavy quark and antiquark respectively. In eq. (3.1), we have made use of the vacuum-saturation approximation to relate the LDMEs for charmonium decay to those for production [5]

$$\langle \mathcal{O}_H \rangle_H = \langle 0 | \chi^\dagger \mathcal{K}_H \psi | H \rangle \langle H | \psi^\dagger \mathcal{K}_H \chi | 0 \rangle \left(1 + \mathcal{O}(v^4) \right), \quad (3.3)$$

where v denotes the typical velocity of the charm quark in charmonium.

In eq. (3.1), the factor $\sqrt{2m_\Upsilon} \sqrt{2m_H}$ appears on the right side because we adopt relativistic normalization for the meson states Υ and H , but we use conventional nonrelativistic normalization for the NRQCD LDMEs. Since we do not consider the relativistic corrections in current work, it is reasonable to take the approximation $m_\Upsilon \approx 2m_b$ and $m_H \approx 2m_c$. In addition, it is straightforward to deduce the helicity selection rule for SDCs

$$c_{\lambda_1, \lambda_2}(H) \propto r^{1/2+|\lambda_1|} \quad (3.4)$$

from (2.4) by noticing that $\sqrt{\langle \mathcal{O}_H \rangle_H} \propto m_c^n$.

Since the NRQCD SDCs are insensitive to the nonperturbative hadronization effects, they can be determined with the aid of the standard perturbative matching technique. That is, by replacing the physical Υ with a fictitious onium $b\bar{b}(^3S_1)$, and replacing H meson with \tilde{H} composed of a free $c\bar{c}$ pair and carrying the same quantum numbers as H , i.e., $\tilde{H} = c\bar{c}(^1S_0)$ for η_c and $\tilde{H} = c\bar{c}(^3P_J)$ for χ_{cJ} . Explicitly, we have

$$\begin{aligned} \mathcal{A}_{\lambda_1, \lambda_2}^{(\tilde{H})} &= c_{\lambda_1, \lambda_2}(H) \frac{\sqrt{\langle b\bar{b}(^3S_1) | \mathcal{O}_\Upsilon | b\bar{b}(^3S_1) \rangle}}{m_b^{3/2}} \frac{\sqrt{\langle \tilde{H} | \mathcal{O}_H | \tilde{H} \rangle}}{m_c^n} \\ &= c_{\lambda_1, \lambda_2}(H) 2N_c \frac{2m_c 2m_b}{m_b^{3/2} m_c^n}, \end{aligned} \quad (3.5)$$

where we use the relativistic normalization for the heavy quark states in the computation of full QCD amplitude $\mathcal{A}_{\lambda_1, \lambda_2}^{(\tilde{H})}$ and NRQCD matrix elements. An additional factor $2N_c$ arises from the spin and color factors of the NRQCD matrix elements.

From eq. (3.5), we are able to reexpress the SDC as

$$c_{\lambda_1, \lambda_2}(H) = \mathcal{A}_{\lambda_1, \lambda_2}^{(\tilde{H})} \frac{m_b^{1/2} m_c^{n-1}}{8N_c}. \quad (3.6)$$

To evaluate the QCD amplitude $\mathcal{A}_{\lambda_1, \lambda_2}^{(\tilde{H})}$, we assign the momenta of the b and \bar{b} quarks to be $\frac{Q}{2}$ and the momenta of the c and \bar{c} quarks to be

$$p = \frac{P}{2} + q, \quad (3.7a)$$

$$\bar{p} = \frac{P}{2} - q, \quad (3.7b)$$

where P and q denote the total momentum of the $c\bar{c}$ pair and the relative momentum, respectively. The on-shell condition $p^2 = \bar{p}^2 = m_c^2$ enforces that

$$P \cdot q = 0, \quad P^2 = 4m_c^2. \quad (3.8)$$

It is convenient to employ the covariant spin-projector and color-projector to enforce the $b\bar{b}$ and $c\bar{c}$ pairs in the spin-singlet/spin-triplet and color-singlet states [28, 29]. The relativistically normalized color-singlet/spin-triplet projector for Υ meson reads

$$\bar{\Pi}_1 = \frac{-1}{\sqrt{2}} \left(\frac{Q}{2} + m_b \right) \not{\epsilon}_\Upsilon \otimes \frac{\mathbf{1}_c}{\sqrt{N_c}}, \quad (3.9)$$

where ϵ_Υ denotes the polarization vector of Υ . The relativistically normalized color-singlet and spin-singlet/spin-triplet projectors for charmonium read [29]

$$\Pi_0 = \frac{1}{8\sqrt{2}m_c^2} (\not{p} - m_c) \gamma^5 (\not{P} + 2m_c) (\not{p} + m_c) \otimes \frac{\mathbf{1}_c}{\sqrt{N_c}}, \quad (3.10a)$$

$$\Pi_1^\mu = \frac{-1}{8\sqrt{2}m_c^2} (\not{p} - m_c) \gamma^\mu (\not{P} + 2m_c) (\not{p} + m_c) \otimes \frac{\mathbf{1}_c}{\sqrt{N_c}}. \quad (3.10b)$$

The amplitude of $b\bar{b}(^3S_1) \rightarrow c\bar{c}(^1S_0) + \gamma$ can be projected out by directly replacing the bottom spinors $u(Q/2)\bar{v}(Q/2)$ with $\bar{\Pi}_1$ and replacing the charm spinors $v(\bar{p})\bar{u}(p)$ with Π_0 , namely

$$\mathcal{A}^{(c\bar{c}(^1S_0))} = \text{Tr}[\bar{\Pi}_1 \mathcal{A} \Pi_0] \Big|_{q=0}, \quad (3.11)$$

where \mathcal{A} represents the quark-level amplitude of $b\bar{b} \rightarrow c\bar{c} + \gamma$ with the external quark spinors truncated. Since we are only concerned with the SDCs at the lowest order in velocity expansion, the relative momentum q is set to zero.

The amplitude of $b\bar{b}(^3S_1) \rightarrow c\bar{c}(^3P_J) + \gamma$ can be projected out by differentiating the color-singlet/spin-triplet quark-level amplitude with respect to the relative momentum q , followed by setting q to zero:

$$\mathcal{A}^{(c\bar{c}(^3P_J))} = \epsilon_{\mu\nu}^{*(J)} \frac{d}{dq_\nu} \text{Tr}[\bar{\Pi}_1 \mathcal{A} \Pi_1^\mu] \Big|_{q=0}, \quad (3.12)$$

with $\epsilon_{\mu\nu}^{(J)}$ denoting the polarization vectors affiliated with $J = 0, 1, 2$.

In order to further extract the helicity amplitudes, it is very useful to construct various helicity projectors $\mathcal{P}_{\lambda_1, \lambda_2}^{(H)}$, the explicit expressions of which can be found in Appendix A. Making use of the helicity projectors, we can readily obtain the helicity amplitudes $\mathcal{A}_{\lambda_1, \lambda_2}^{(\tilde{H})}$

through first replacing the polarization vectors of Υ and H with the corresponding $\mathcal{P}_{\lambda_1, \lambda_2}^{(H)}$, and then contracting the Lorentz indices.

Now we have collected all the necessary ingredients to evaluate the quark-level helicity amplitudes $\mathcal{A}_{\lambda_1, \lambda_2}^{(\tilde{H})}$ in perturbative QCD. It is then straightforward to ascertain the SDCs following eq. (3.6), and further compute the physical helicity amplitudes (3.1) and partial widths (2.1).

4 Technical strategy of calculating SDCs

In this section, we describe the computational technicalities utilized in evaluating the QCD amplitude and the SDCs.

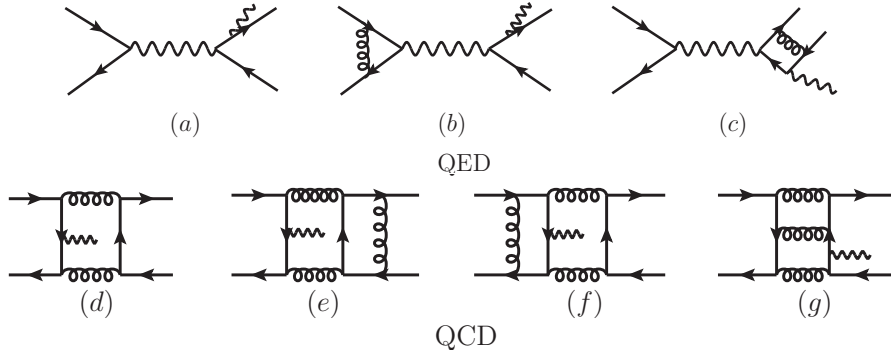


Figure 1. Some representative Feynman diagrams for $\Upsilon \rightarrow \eta_c(\chi_{cJ}) + \gamma$. (a) corresponds to the LO QED contribution, (b) and (c) correspond to the NLO QED contribution, (d) corresponds to the LO QCD contribution, and (e)-(g) correspond to the NLO QCD contribution. The Feynman diagrams are drawn by JaxoDraw [30].

We use **FeynArts** [31] to generate the Feynman diagrams for $b\bar{b} \rightarrow c\bar{c} + \gamma$ and corresponding Feynman amplitudes through NLO in α_s . Some typical QED and QCD Feynman diagrams are illustrated in figure 1. Due to the color-singlet constraint and C-parity conservation, the QCD Feynman diagrams start at one-loop order. In this work, we will compute both contributions through relative order $\mathcal{O}(\alpha_s)$, *i.e.*, calculating the QED contribution through one-loop order and QCD contribution through two-loop order. Employing the color-singlet/spin-triplet projectors (3.9) and (3.10), following the recipe as depicted in section 3 to single out the S or P -wave components of the amplitude, we are able to project out the intended $b\bar{b}(^3S_1) \rightarrow c\bar{c}(^1S_0/^3P_J) + \gamma$ amplitude, order by order in α_s . We then employ the packages **FeynCalc** [32, 33] and **FormLink** [34] to carry out various helicity amplitudes with the aid of the helicity projectors specified in Appendix A.

It is quite straightforward to compute the LO QED SDCs, which will be analytically presented in section 6. To determine the SDCs at loop level, we adopt the standard approach to directly extract the SDCs, *i.e.*, we implement the procedures (3.11) for η_c and (3.12) for χ_{cJ} prior to conducting the loop integral, which amounts to directly extracting the contribution from the hard region in the context of strategy of region [35]. We apply the dimensional regularization to regularize both UV and IR divergences throughout this

work. For the loop integrals, we utilize the packages **Apart** [36] and **FIRE** [37] to conduct partial fraction and the corresponding integration-by-part (IBP) reduction. We end up with 13 one-loop master integrals (MIs) and 567 two-loop MIs, of which 237 are complex-valued integrals. For the one-loop MIs, one can work out the analytical expressions with the aid of **Package-X** [38].

It becomes rather challenging to deduce the analytical expressions for all the encountered two-loop MIs. Instead, we are content with high-precision numerical results which actually are enough for the phenomenological analysis. For the two-loop MIs, we make use of the **FIESTA** [39] to perform sector decomposition (SD), which are initially introduced in Refs. [40–45]. For the real-valued MIs, we directly use **CubPack** [46] to carry out the numerical integration. In contrast to the application of SD to the Euclidean region, the singularities encountered in the physical region lie inside, rather than sit on, the integration boundary, which render the integrals hard to be numerically evaluated. We can overcome the difficulty by deforming the integration contour through the following variable transformation [47]:

$$z_k = x_k - i\lambda_k x_k(1 - x_k) \frac{\partial F}{\partial x_k}, \quad (4.1)$$

where F denotes the F -term in the α parametrization, λ_k is some positive number. Actually, the integration efficiency may vary drastically with λ_k . In our calculation, we first choose a set of λ_k and utilize **CubPack** to conduct the first-round rough numerical integration. For those integrals with large estimated errors, we adjust the values of λ_k and perform the integration with a fixed number of sample points. The operation will be repeated until we find a relatively optimized values of λ_k , which render the integration error endurable. With the new determined λ_k , the integral will be evaluated once again with the aid of a parallelized integrator **HCubature** [48] to reach the desired precision. For more technical detail, we refer the readers to Ref. [20]. In very rare case, the integrator may generate finite however incorrect numerical results for some integrals because of the relatively large λ_k , which actually reverses the sign of the imaginary part of the F -term. This difficulty can be overcome by decreasing the values of λ_k through a multiplication factor (less than 1), and reevaluating the integration.

To eliminate the UV divergences at NLO, we perform the renormalization procedure by implementing the $\mathcal{O}(\alpha_s)$ expressions of the renormalization constants Z_2 and Z_m accurate up to $\mathcal{O}(\epsilon)$, which can be found in Refs. [49–51].

To guarantee the correctness of the two-loop calculation, we make the following check. We recalculate all the real-valued MIs through another public package **pySecDec** [52]. Meanwhile, we reevaluate most of the complex-valued two-loop MIs (215 of total 237 MIs), which can be converted into real-valued MIs through the Cheng-Wu theorem [53–55]. The approach of using Cheng-Wu theorem to deal with loop integrals makes the numerical integration much efficient, and the technical description is presented in Appendix B. The values of the reevaluated MIs are consistent with those computed by **FIESTA** within the errors. In addition, by using the values of the same sets of MIs, all the divergences in the 7 helicity channels can be removed by the renormalization constants.

5 Two schemes to deal with the QED contribution

As illustrated in figure 1, there are two kinds of Feynman diagrams for the processes $\Upsilon \rightarrow H + \gamma$: QED Feynman diagrams represented by figure 1(a)-(c), and QCD Feynman diagrams represented by figure 1(d)-(g). Correspondingly, we can split the SDCs into two parts

$$c_{\lambda_1, \lambda_2}(H) = d_{\lambda_1, \lambda_2}(H) + f_{\lambda_1, \lambda_2}(H), \quad (5.1)$$

where $d_{\lambda_1, \lambda_2}(H)$ and $f_{\lambda_1, \lambda_2}(H)$ correspond to the contributions from the QED Feynman diagrams and the QCD Feynman diagrams respectively.

It is well known, when computing a vector heavy quarkonium decay into a virtual photon, one confronts very poor convergence in perturbative expansion [10–12]. Since there exists the similar structure in the QED Feynman diagrams of $\Upsilon \rightarrow H + \gamma$, one may worry whether the higher order perturbative corrections will significantly change the theoretical prediction for the QED contribution. Actually, we can reduce the theoretical uncertainty by replacing the contribution of $\Upsilon \rightarrow \gamma^*$ in the QED amplitude by the Υ decay constant [56].

The Υ decay constant is defined through the following matrix element of the electromagnetic current

$$\langle \Upsilon(\epsilon) | \bar{b} \gamma^\mu b | 0 \rangle = -f_\Upsilon m_\Upsilon \epsilon_\Upsilon^{*\mu}, \quad (5.2)$$

where the state of Υ meson is relativistically renormalized, and we adopt the same sign convention as in Ref. [56]. The decay constant f_Υ can be related to the Υ electromagnetic decay width through

$$\Gamma(\Upsilon \rightarrow e^+ e^-) = \frac{4\pi}{3m_\Upsilon} \alpha^2 e_b^2 f_\Upsilon^2, \quad (5.3)$$

where α signifies the electromagnetic coupling constant and $e_b = -1/3$ denotes the charge of bottom quark. It is straightforward to derive

$$f_\Upsilon = \sqrt{\frac{3m_\Upsilon \Gamma(\Upsilon \rightarrow e^+ e^-)}{4\pi \alpha^2 e_b^2}}. \quad (5.4)$$

To make distinguishment, we refer to the factorization formula expressed in eq. (3.1) as QED_I scheme, while the approach by replacing $\Upsilon \rightarrow \gamma^*$ with the decay constant f_Υ as QED_{II} scheme. Actually, we can easily convert the QED_I scheme to the QED_{II} scheme by making use of the following substitution

$$\sqrt{\langle \mathcal{O}_\Upsilon \rangle_\Upsilon} \rightarrow \sqrt{m_b} f_\Upsilon, \quad (5.5)$$

meanwhile, removing the contributions from the Feynman diagram figure 1(b) in the NLO computation. For clarity, it is necessary to rewrite the factorization for the QED helicity amplitude in the QED_{II} scheme:

$$\left(A_{\lambda_1, \lambda_2}^{(H)} \right)_{\text{QED}_{\text{II}}} = \sqrt{2m_\Upsilon} \sqrt{2m_H} d_{\lambda_1, \lambda_2}(H) \frac{f_\Upsilon}{m_b} \frac{\sqrt{\langle \mathcal{O}_H \rangle_H}}{m_c^n}. \quad (5.6)$$

We will make more discussions about the two schemes in section 6 and section 7.

6 Main results

In this section, we present the analytical expressions for the LO QED helicity SDCs and the numerical expressions for all other SDCs though NLO in α_s . It is convenient to expand the QED and QCD helicity SDCs $d_{\lambda_1, \lambda_2}(H)$ and $f_{\lambda_1, \lambda_2}(H)$ defined in (5.1) in powers of the strong coupling constant:

$$d_{\lambda_1, \lambda_2}(H) = e^3 \left[d_{\lambda_1, \lambda_2}^{(0)}(H) + \frac{\alpha_s}{\pi} d_{\lambda_1, \lambda_2}^{(1)}(H) + \mathcal{O}(\alpha_s^2) \right], \quad (6.1)$$

where e denotes the unit of electric charge, and

$$f_{\lambda_1, \lambda_2}(H) = e\alpha_s^2 \left[f_{\lambda_1, \lambda_2}^{(0)}(H) + \frac{\alpha_s}{\pi} \left(\frac{1}{2} \beta_0 \ln \frac{\mu_R^2}{m_b^2} f_{\lambda_1, \lambda_2}^{(0)}(H) + f_{\lambda_1, \lambda_2}^{(1)}(H) \right) + \mathcal{O}(\alpha_s^2) \right], \quad (6.2)$$

where $\beta_0 = (11/3)C_A - (4/3)T_F n_f$ is the one-loop coefficient of the QCD β function, with $T_F = \frac{1}{2}$ and n_f signifying the number of active quark flavors. In this work, we take $n_f = n_L + n_H$, where $n_L = 3$ labels the number of light quark flavors and $n_H = 1$ indicates the number of heavy quark flavors. The occurrence of the $\beta_0 \ln \mu_R^2$ in (6.2) simply reflects the renormalization group invariance.

$d_{\lambda_1, \lambda_2}^{(0)}(H)$ are easy to evaluate and read

$$d_{0,1}^{(0)}(\eta_c) = -\frac{r^{1/2}}{27}, \quad (6.3a)$$

$$d_{0,1}^{(0)}(\chi_{c0}) = \frac{(1 - 3r^2)r^{1/2}}{27\sqrt{3}(1 - r^2)}, \quad (6.3b)$$

$$d_{1,1}^{(0)}(\chi_{c1}) = \frac{-\sqrt{2}r^{3/2}}{27(1 - r^2)}, \quad d_{0,1}^{(0)}(\chi_{c1}) = \frac{\sqrt{2}r^{1/2}}{27(1 - r^2)}, \quad (6.3c)$$

$$d_{2,1}^{(0)}(\chi_{c2}) = \frac{-2r^{5/2}}{27(1 - r^2)}, \quad d_{1,1}^{(0)}(\chi_{c2}) = \frac{\sqrt{2}r^{3/2}}{27(1 - r^2)}, \quad d_{0,1}^{(0)}(\chi_{c2}) = \frac{-\sqrt{6}r^{1/2}}{81(1 - r^2)}, \quad (6.3d)$$

which manifestly satisfy the helicity selection rule (3.4). It is also not hard to compute $d_{\lambda_1, \lambda_2}^{(1)}(H)$. Actually, the explicit expressions of $d_{\lambda_1, \lambda_2}^{(1)}(H)$ can be obtained by combining the results of the $\mathcal{O}(\alpha_s)$ corrections to $\Upsilon \rightarrow \gamma^*$ and $\gamma^* \rightarrow \eta_c(\chi_{cJ}) + \gamma$, the analytical expressions of which can be respectively found in Ref [5] and Ref. [57].

It is necessary to discuss the difference between the QED SDCs in the two QED schemes introduced in section 5. It is obvious that the LO SDCs $d_{\lambda_1, \lambda_2}^{(0)}(H)$ are equal in the QED_I and QED_{II} schemes. On the other hand, since all the radiative corrections to $\Upsilon \rightarrow \gamma^*$ are encoded in the decay constant, we must remove the QCD corrections to $\Upsilon \rightarrow \gamma^*$ from $d_{\lambda_1, \lambda_2}^{(1)}(H)$ in the QED_{II} scheme. It is straightforward to derive

$$\left(d_{\lambda_1, \lambda_2}^{(1)}(H) \right)_{\text{QED}_{\text{II}}} = \left(d_{\lambda_1, \lambda_2}^{(1)}(H) \right)_{\text{QED}_{\text{I}}} + 2C_F d_{\lambda_1, \lambda_2}^{(0)}(H), \quad (6.4)$$

where the second term on the right side stems from the well-known NLO QCD corrections to $\Upsilon \rightarrow \gamma^*$. In the next section, we will evaluate the partial widths of each helicity in the two schemes and make comparison.

The QCD contribution for $\Upsilon \rightarrow H + \gamma$ starts at one-loop order. The LO SDCs $f_{\lambda_1, \lambda_2}^{(0)}(H)$ can be evaluated analytically with the aid of the **Package-X**. Very recently, the analytical expressions of the decay widths at LO for the processes $\Upsilon \rightarrow H + \gamma$ were presented in terms of the one-loop scalar Passarino-Veltman integrals in Ref. [7]. Since the analytical expressions are rather lengthy and cumbersome, we suppress the explicit forms of $f_{\lambda_1, \lambda_2}^{(0)}(H)$ in this work. Instead, we present the numerical results. As mentioned, it is rather challenging to compute $f_{\lambda_1, \lambda_2}^{(1)}(H)$ analytically, so we evaluate their values numerically.

To make numerical computation, we choose two sets of typical values of the bottom mass and charm mass, i.e., $m_c = 1.483 \text{ GeV}$, $m_b = 4.580 \text{ GeV}$ and $m_c = 1.68 \text{ GeV}$, $m_b = 4.78 \text{ GeV}$, which correspond to the one-loop and the two-loop heavy quark pole masses respectively [14, 22, 56], converted from the $\overline{\text{MS}}$ masses $\overline{m}_c = 1.28 \text{ GeV}$ and $\overline{m}_b = 4.18 \text{ GeV}$.

Table 1. NRQCD predictions on the dimensionless helicity SDCs for $m_c = 1.483 \text{ GeV}$ and $m_b = 4.580 \text{ GeV}$. The QED SDCs are evaluated in the QED_{II} scheme. The errors in $f_{\lambda_1, \lambda_2}^{(1)}$ originate from numerical computation.

$m_c = 1.483 \text{ GeV}, m_b = 4.580 \text{ GeV} ; \text{ SDCs}(\times 10^{-2})$					
H	helicity	QCD		QED _{II}	
		$f_{\lambda_1, \lambda_2}^{(0)}$	$f_{\lambda_1, \lambda_2}^{(1)}$	$d_{\lambda_1, \lambda_2}^{(0)}$	$d_{\lambda_1, \lambda_2}^{(1)}$
η_c	$\lambda_1 = 0, \lambda_2 = 1$	$-15.14 - 6.33i$	$-70.0(3) - 116.5(2)i$ $+(6.78 + 9.02i)n_L + (5.11 + 4.76i)n_H$	-2.11	$3.04 + 2.80i$
χ_{c0}	$\lambda_1 = 0, \lambda_2 = 1$	$-13.56 + 10.97i$	$-43.5(8) + 62.9(6)i$ $+(25.16 - 3.53i)n_L + (12.48 - 8.24i)n_H$	0.93	$1.35 + 1.47i$
χ_{c1}	$\lambda_1 = 1, \lambda_2 = 1$	-4.62	$-26.6(2) - 17.1(2)i$ $+(2.00 + 0.11i)n_L + 1.13n_H$	-1.08	$1.72 + 1.43i$
	$\lambda_1 = 0, \lambda_2 = 1$	17.89	$64.4(4) + 45.0(4)i$ $+(-11.45 - 1.26i)n_L - 6.32n_H$	3.33	$-6.27 - 3.75i$
χ_{c2}	$\lambda_1 = 2, \lambda_2 = 1$	$-0.67 + 6.11i$	$33.8(3) - 3.2(2)i$ $+(5.55 - 6.09i)n_L + (1.80 - 4.60i)n_H$	-0.49	$2.31 - 0.86i$
	$\lambda_1 = 1, \lambda_2 = 1$	$0.43 - 9.84i$	$-24.0(3) - 8.3(3)i$ $+(-8.00 + 9.15i)n_L + (-2.61 + 7.40i)n_H$	1.08	$-5.35 + 2.67i$
	$\lambda_1 = 0, \lambda_2 = 1$	$0.15 + 15.93i$	$21.6(5) + 14.6(4)i$ $+(11.66 - 14.64i)n_L + (3.65 - 11.98i)n_H$	-1.92	$8.22 - 2.44i$

Our main results of the SDCs $d_{\lambda_1, \lambda_2}^{(0)}(H)$, $d_{\lambda_1, \lambda_2}^{(1)}(H)$, $f_{\lambda_1, \lambda_2}^{(0)}(H)$ and $f_{\lambda_1, \lambda_2}^{(1)}(H)$ are tabulated in table 1 for $m_c = 1.483 \text{ GeV}, m_b = 4.580 \text{ GeV}$ and in table 2 for $m_c = 1.68 \text{ GeV}, m_b = 4.78 \text{ GeV}$. In the tables, the QED SDCs are evaluated in the QED_{II} scheme. Actually, it is straightforward to convert the values of $d_{\lambda_1, \lambda_2}^{(1)}$ in the tables into those in the QED_{I} scheme by utilizing the formula (6.4). For the sake of reference, we keep the explicit n_L and n_H dependence in the SDCs.

We have two observations from the tables. First, the LO SDCs $f_{\lambda_1, \lambda_2}^{(0)}(\chi_{c1})$ do not have imaginary parts, which can be well understood by invoking the Cutkosky rule and by noticing the process $\chi_{c1} \rightarrow 2\text{gluons}$ is strictly forbidden by the Yang's theorem. Similarly, the imaginary parts of the terms proportional to n_H in $f_{\lambda_1, \lambda_2}^{(1)}(\chi_{c1})$ are also absent, which can be explained by the Yang's theorem and the degenerate phase space for $\chi_{c1} \rightarrow c\bar{c} + \text{gluon}$.

Table 2. NRQCD predictions on the dimensionless helicity SDCs for $m_c = 1.68$ GeV and $m_b = 4.78$ GeV. We use the same conventions as table 1.

$m_c = 1.68$ GeV, $m_b = 4.78$ GeV ; SDCs($\times 10^{-2}$)					
H	helicity	QCD		QED _{II}	
		$f_{\lambda_1, \lambda_2}^{(0)}$	$f_{\lambda_1, \lambda_2}^{(1)}$	$d_{\lambda_1, \lambda_2}^{(0)}$	$d_{\lambda_1, \lambda_2}^{(1)}$
η_c	$\lambda_1 = 0, \lambda_2 = 1$	$-15.46 - 7.24i$	$-65.9(2) - 126.5(2)i$ $+(6.27 + 9.85i)n_L + (4.69 + 5.04i)n_H$	-2.20	$3.38 + 2.81i$
χ_{c0}	$\lambda_1 = 0, \lambda_2 = 1$	$-13.38 + 12.54i$	$-40.6(4) + 78.2(3)i$ $+(25.35 - 4.57i)n_L + (11.95 - 8.74i)n_H$	0.91	$1.62 + 1.64i$
χ_{c1}	$\lambda_1 = 1, \lambda_2 = 1$	-5.30	$-27.8(2) - 19.0(2)i$ $+(2.45 + 0.20i)n_L + 1.28n_H$	-1.25	$2.16 + 1.57i$
	$\lambda_1 = 0, \lambda_2 = 1$	18.38	$63.3(5) + 46.3(5)i$ $+(-11.71 - 1.46i)n_L - 6.08n_H$	3.54	$-7.09 - 3.69i$
χ_{c2}	$\lambda_1 = 2, \lambda_2 = 1$	$-1.17 + 6.84i$	$35.0(2) - 4.7(2)i$ $+(6.62 - 6.22i)n_L + (2.24 - 4.77i)n_H$	-0.62	$2.85 - 1.10i$
	$\lambda_1 = 1, \lambda_2 = 1$	$1.22 - 10.53i$	$-24.1(4) - 4.3(4)i$ $+(-9.32 + 8.97i)n_L + (-3.21 + 7.34i)n_H$	1.25	$-6.02 + 3.08i$
	$\lambda_1 = 0, \lambda_2 = 1$	$-1.09 + 15.88i$	$19.9(5) + 5.9(5)i$ $+(12.89 - 13.40i)n_L + (4.35 - 10.07i)n_H$	-2.05	$8.68 - 2.79i$

Second, we find the LO QCD SDCs of χ_{c1} roughly satisfy the helicity selection rule, *i.e.*, $|f_{1,1}^{(0)}| \ll |f_{0,1}^{(0)}|$. However, the helicity selection rule is not so manifest for the counterparts of χ_{c2} , which may be partly due to the fact that the mass of bottom quark is not much larger than that of charm quark.

7 Phenomenology and discussion

In this section, we apply the formulas and the numerical results obtained in section 3 and section 6 to make concrete phenomenological analysis. Prior to making predictions, we need to fix the various input parameters. We take the QED running coupling constant evaluated at mass of Υ meson, $\alpha(m_\Upsilon) = \frac{1}{131}$. The QCD running coupling constant at different renormalization scales is evaluated with the aid of the package RunDec [58].

We take the masses of the bottomonium and charmonia

$$m_\Upsilon = 9.4603 \text{ GeV}, \quad m_{\eta_c} = 2.9839 \text{ GeV}, \quad (7.1a)$$

$$m_{\chi_{c0}} = 3.41471 \text{ GeV}, \quad m_{\chi_{c1}} = 3.51067 \text{ GeV}, \quad m_{\chi_{c2}} = 3.55617 \text{ GeV}, \quad (7.1b)$$

and the full Υ decay width $\Gamma_\Upsilon = 54.02 \pm 1.25 \text{ keV}$ from the latest particle data group (PDG) [59]. In addition, the Υ decay constant $f_\Upsilon = 683.8 \pm 4.6 \text{ MeV}$ is determined through eq. (5.4).

The NRQCD LDMEs for quarkonia have been obtained through various methods, *i.e.*, by fitting experimental data [60, 61], by lattice computation [62–64], and by computation based on the nonrelativistic effective field theories [65]. For more discussion, we refer the readers to Ref. [65] and the references therein. In this work, we approximate the NRQCD

LDMs for S -wave and P -wave quarkonia by the Schrödinger radial wave function at origin and first derivative of the Schrödinger radial wave function at origin respectively,

$$\langle \mathcal{O}_\Upsilon \rangle_\Upsilon \approx \frac{N_c}{2\pi} |R_{1S}^{b\bar{b}}(0)|^2 = \frac{N_c}{2\pi} \times 6.477 \text{ GeV}^3, \quad (7.2a)$$

$$\langle \mathcal{O}_{\eta_c} \rangle_{\eta_c} \approx \frac{N_c}{2\pi} |R_{1S}^{c\bar{c}}(0)|^2 = \frac{N_c}{2\pi} \times 0.81 \text{ GeV}^3, \quad (7.2b)$$

$$\langle \mathcal{O}_{\chi_{cJ}} \rangle_{\chi_{cJ}} \approx \frac{3N_c}{2\pi} |R_{2P}^{c\bar{c}}(0)|^2 = \frac{3N_c}{2\pi} \times 0.075 \text{ GeV}^5, \quad (7.2c)$$

where $N_c = 3$ signifies the number of color, and we take the values of the radial wave functions from Ref. [66], which are evaluated based on the Buchmüller-Tye (BT) potential model and are frequently used in phenomenological study.

With all these input parameters, we can evaluate the helicity decay widths by eq. (2.1) and the total decay widths by eq. (2.5). The branching fractions can be immediately obtained through dividing the decay widths by the full decay width Γ_Υ . We tabulate the NRQCD predictions on the helicity partial widths and branching fractions of $\Upsilon \rightarrow H + \gamma$ in table 3 for $m_c = 1.483 \text{ GeV}$, $m_b = 4.580 \text{ GeV}$, and in table 4 for $m_c = 1.68 \text{ GeV}$, $m_b = 4.78 \text{ GeV}$. To facilitate the comparison, we use the symbols Γ_{QCD} and Γ_{total} to represent the pure QCD contribution and the total contribution respectively. The uncertainties affiliated with the decay widths and the branching fractions are estimated by varying the renormalization scale μ_R from $2m_c$ to $2m_b$, with the central values evaluated at $\mu_R = m_b$. In addition, we include the uncertainties from Γ_Υ and f_Υ in the branching fractions.

Table 3. NRQCD predictions on the helicity decay widths and branching fractions of $\Upsilon \rightarrow H + \gamma$ at LO and NLO in α_s for $m_c = 1.483 \text{ GeV}$ and $m_b = 4.580 \text{ GeV}$. The LDMs are evaluated through the BT potential model. Γ_{QCD} represents the pure QCD contribution, and Γ_{total} denotes the sum of QCD, QED and the interference, where we compute the QED contribution in the QED_{II} scheme. We include the uncertainties from the renormalization scale in both the decay widths and the branching fractions. In addition, we also include the uncertainties (the second entry) originating from Γ_Υ and f_Υ .

$m_c = 1.483 \text{ GeV}, m_b = 4.580 \text{ GeV} ; \quad \Gamma(\times 10^{-1} \text{ eV})$							
H	helicity	LO			NLO		
		Γ_{QCD}	Γ_{total}	$\text{Br}(\times 10^{-5})$	Γ_{QCD}	Γ_{total}	$\text{Br}(\times 10^{-5})$
η_c	$\lambda_1 = 0, \lambda_2 = 1$	$12.66^{+8.44}_{-6.05}$	$18.91^{+10.05}_{-7.59}$	$7.00^{+3.72+0.12}_{-2.81-0.11}$	$22.09^{+3.53}_{-5.34}$	$28.27^{+3.44}_{-5.70}$	$10.47^{+1.27+0.18}_{-2.11-0.17}$
χ_{c0}	$\lambda_1 = 0, \lambda_2 = 1$	$1.74^{+1.16}_{-0.83}$	$1.49^{+1.08}_{-0.76}$	$0.55^{+0.40+0.009}_{-0.28-0.009}$	$1.75^{+0.002}_{-0.17}$	$1.57^{+0.01}_{-0.19}$	$0.58^{+0.003+0.01}_{-0.07-0.009}$
χ_{c1}	$\lambda_1 = 1, \lambda_2 = 1$	$0.12^{+0.08}_{-0.05}$	$0.25^{+0.11}_{-0.09}$	$1.31^{+0.62+0.02}_{-0.48-0.01}$	$0.21^{+0.03}_{-0.05}$	$0.34^{+0.03}_{-0.06}$	$1.44^{+0.02+0.02}_{-0.16-0.02}$
	$\lambda_1 = 0, \lambda_2 = 1$	$1.82^{+1.21}_{-0.87}$	$3.28^{+1.57}_{-1.22}$		$2.20^{+0.04}_{-0.32}$	$3.54^{+0.03}_{-0.37}$	
χ_{c2}	$\lambda_1 = 2, \lambda_2 = 1$	$0.21^{+0.14}_{-0.10}$	$0.23^{+0.14}_{-0.10}$	$0.86^{+0.54+0.01}_{-0.39-0.01}$	$0.15^{+0.02}_{-0.01}$	$0.13^{+0.01}_{-0.001}$	$0.53^{+0.04+0.009}_{-0.12-0.008}$
	$\lambda_1 = 1, \lambda_2 = 1$	$0.55^{+0.37}_{-0.26}$	$0.58^{+0.37}_{-0.27}$		$0.42^{+0.01}_{-0.05}$	$0.35^{+0.02}_{-0.07}$	
	$\lambda_1 = 0, \lambda_2 = 1$	$1.44^{+0.96}_{-0.69}$	$1.50^{+0.96}_{-0.69}$		$1.08^{+0.04}_{-0.20}$	$0.96^{+0.07}_{-0.25}$	

Comparing table 3 with table 4, we find the partial widths for $m_c = 1.483 \text{ GeV}, m_b = 4.580 \text{ GeV}$ are a bit larger than those for $m_c = 1.68 \text{ GeV}, m_b = 4.78 \text{ GeV}$. It is mainly due to the fact that the helicity amplitude is inversely proportional to the heavy quark

Table 4. NRQCD predictions on the helicity decay widths and branching fractions of $\Upsilon \rightarrow H + \gamma$ at LO and NLO in α_s for $m_c = 1.68$ GeV and $m_b = 4.78$ GeV. We use the same conventions as in table 4.

$m_c = 1.68 \text{ GeV}, m_b = 4.78 \text{ GeV} ; \quad \Gamma(\times 10^{-1} \text{ eV})$							
H	helicity	LO			NLO		
		Γ_{QCD}	Γ_{total}	$\text{Br}(\times 10^{-5})$	Γ_{QCD}	Γ_{total}	$\text{Br}(\times 10^{-5})$
η_c	$\lambda_1 = 0, \lambda_2 = 1$	$9.37^{+4.65}_{-4.44}$	$14.16^{+5.59}_{-5.59}$	$5.24^{+2.07+0.09}_{-2.07-0.08}$	$16.34^{+2.17}_{-3.88}$	$20.97^{+2.13}_{-4.15}$	$7.76^{+0.79+0.13}_{-1.52-0.12}$
χ_{c0}	$\lambda_1 = 0, \lambda_2 = 1$	$1.03^{+0.51}_{-0.49}$	$0.89^{+0.48}_{-0.45}$	$0.33^{+0.18+0.006}_{-0.17-0.005}$	$1.12^{+0.01}_{-0.136}$	$1.03^{+0.02}_{-0.15}$	$0.38^{+0.007+0.006}_{-0.05-0.006}$
χ_{c1}	$\lambda_1 = 1, \lambda_2 = 1$	$0.09^{+0.04}_{-0.04}$	$0.18^{+0.06}_{-0.06}$	$0.78^{+0.27+0.011}_{-0.28-0.011}$	$0.13^{+0.01}_{-0.03}$	$0.23^{+0.01}_{-0.04}$	$0.84^{+0.01+0.013}_{-0.03-0.012}$
	$\lambda_1 = 0, \lambda_2 = 1$	$1.02^{+0.51}_{-0.48}$	$1.93^{+0.68}_{-0.69}$		$1.21^{+0.02}_{-0.17}$	$2.03^{+0.01}_{-0.19}$	
χ_{c2}	$\lambda_1 = 2, \lambda_2 = 1$	$0.15^{+0.07}_{-0.07}$	$0.16^{+0.07}_{-0.07}$	$0.51^{+0.23+0.008}_{-0.23-0.008}$	$0.10^{+0.002}_{-0.002}$	$0.08^{+0.005}_{-0.004}$	$0.28^{+0.029+0.005}_{-0.056-0.005}$
	$\lambda_1 = 1, \lambda_2 = 1$	$0.34^{+0.17}_{-0.16}$	$0.37^{+0.17}_{-0.17}$		$0.24^{+0.01}_{-0.03}$	$0.20^{+0.02}_{-0.04}$	
	$\lambda_1 = 0, \lambda_2 = 1$	$0.76^{+0.38}_{-0.36}$	$0.84^{+0.38}_{-0.37}$		$0.53^{+0.03}_{-0.09}$	$0.48^{+0.05}_{-0.11}$	

masses, which can be noted in eq. (3.1). From the tables, we notice the $\mathcal{O}(\alpha_s)$ corrections to the branching fractions are moderate for η_c and χ_{c2} , and have minor effects for the χ_{c0} or χ_{c1} , which indicates the perturbative expansion in α_s exhibits a decent convergent behavior. In addition, we note the partial widths are dominated by the QCD contributions for χ_{c0} and χ_{c2} . In contrast, the QED part contributes considerably to the partial widths of η_c and χ_{c1} , and therefore is indispensable. Moreover, it is interesting to note that the total partial width of η_c is much larger than those of χ_{cJ} , which is mainly caused by the NRQCD LDMEs. The relatively large branching fraction for the process $\Upsilon \rightarrow \eta_c + \gamma$ can provide a good opportunity for experimental search. Among χ_{cJ} productions, we find the partial width of χ_{c1} is several times larger than those of $\chi_{c0,2}$. Actually, we have the similar observations in $e^+e^- \rightarrow \chi_{cJ} + \gamma$, where the production cross section of χ_{c1} is much larger than the others [22]. Finally, it is impressive to observe the renormalization scale dependence in the NLO partial widths and branching fractions are considerably reduced compared to their LO counterparts, especially for χ_{cJ} production.

Recently, Belle collaboration had measured the branching fraction $\text{Br}(\Upsilon \rightarrow \chi_{c1} + \gamma) = 4.7^{+2.4+0.4}_{-1.8-0.5} \times 10^{-5}$, where the two uncertainties correspond to statistical error and systematical error respectively [4]. It is quite disquieting to find the theoretical prediction with $m_c = 1.483$ GeV and $m_b = 4.58$ GeV are only half of the lower bound of the experimental data. Actually, the theoretical predictions are sensitive to the NRQCD LDMEs. Relatively large LDMEs can alleviate the tension between theory and experiment. In addition, the theoretical predictions depend on the heavy quark masses. One may increase the theoretical predictions through decreasing the heavy quark masses. However, the values of the charm and bottom masses may be tuned to be unreliable if we want to explain the experimental measurement. More seriously, we find the NRQCD prediction on the branching fraction of $\Upsilon \rightarrow \eta_c + \gamma$ is several times larger than the experimental upper limit $\text{Br}(\Upsilon \rightarrow \eta_c + \gamma) < 2.9 \times 10^{-5}$ [4]. In addition, we note that the branching fraction for χ_{c1} production is larger than the upper limit of η_c production. Since the configuration of the Feynman diagrams for χ_{c1} is the same as that for η_c , it is rather unexpected that

the production rate for the P-wave χ_{c1} is larger than that for the S-wave η_c . There may exist some underlying mechanism which leads to the unexpectation. Actually, we notice that there is some confliction on $\text{Br}(\Upsilon \rightarrow \chi_{c1} + \gamma)$ between the measurement from Ref. [4] and the measurement from Ref. [1]. Undoubtedly, the discrepancy between theory and experiment deserves further research efforts.

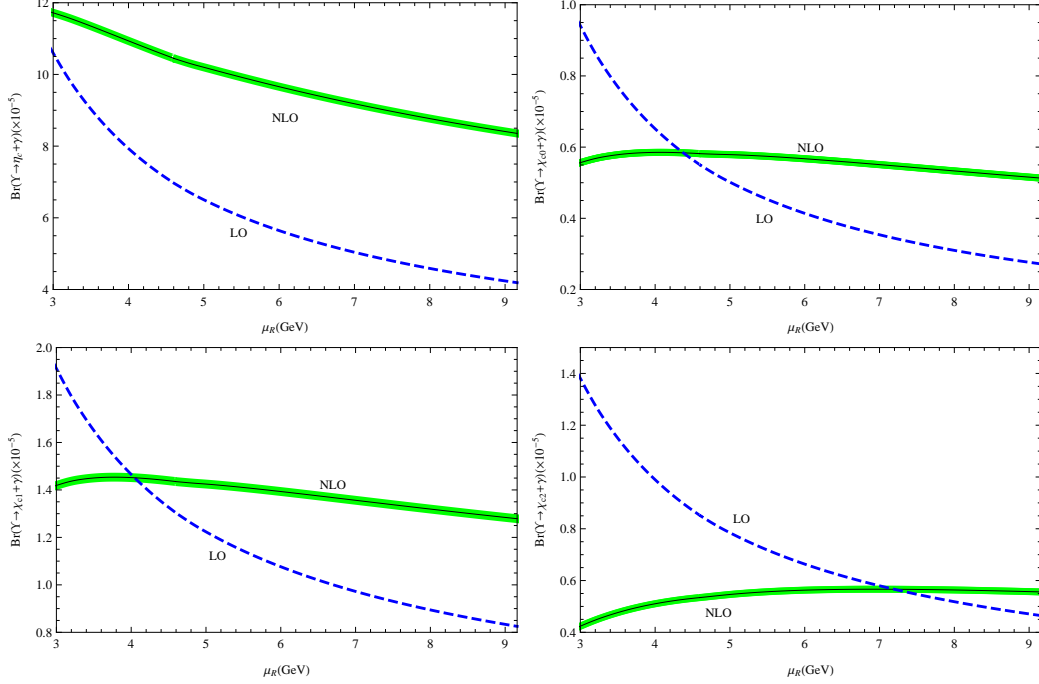


Figure 2. NRQCD predictions for $\text{Br}(\Upsilon \rightarrow H + \gamma)$ as a function of μ_R accurate up to the LO and NLO in α_s . The values of the LDMEs are evaluated through the BT potential model. We take $m_c = 1.483$ GeV and $m_b = 4.58$ GeV. The green band represents the uncertainty band from Γ_Υ and f_Υ .

To closely examine the scale dependence, we display the branching fractions of $\Upsilon \rightarrow H + \gamma$ as a function of the renormalization scale μ_R in figure 2, where we have taken $m_c = 1.483$ GeV, $m_b = 4.580$ GeV. The green band labeled with “NLO” corresponds to the uncertainties from Γ_Υ and f_Υ , which are actually rather small. We find that the NLO prediction exhibits a very mild μ_R -dependence for χ_{c0} and χ_{c1} . The feature, to some extent, reflects a decent perturbative convergent behavior. The NLO prediction can considerably improve the μ_R -dependence for χ_{c2} . In contrast, we note that the NLO prediction seems to only slightly reduce μ_R -dependence compared to the LO prediction for η_c production, which may be attributed to the sizeable α_s corrections to the QCD contribution of η_c .

In section 5, we have introduced two different schemes to deal with the QED contribution. It is interesting to compare the decay widths of the two schemes. The results are illustrated in table 5. We find that the discrepancy between the predictions of the two schemes is quite insubstantial. Even for η_c and χ_{c1} production, where the QED contributions are considerable, the discrepancy is rather negligible. It might indicate the fact that the NRQCD predictions for the process $\Upsilon \rightarrow e^+e^-$ at lower order in α_s can well describe

Table 5. Comparison on the decay widths between the two QED schemes. The decay widths include the contributions from QCD, QED, and the interference. In $\Gamma_{\text{QCD+QED}_\text{I}}$, the QED related contributions are computed in the QED_I scheme, and in $\Gamma_{\text{QCD+QED}_\text{II}}$, the QED related contributions are computed in the QED_{II} scheme. We estimate the uncertainties by sliding μ_R from $2m_c$ to $2m_b$.

$m_c = 1.483 \text{ GeV}, m_b = 4.580 \text{ GeV} ; \quad \Gamma (\times 10^{-1} \text{ eV})$					
H	helicity	LO		NLO	
		$\Gamma_{\text{QCD+QED}_\text{I}}$	$\Gamma_{\text{QCD+QED}_\text{II}}$	$\Gamma_{\text{QCD+QED}_\text{I}}$	$\Gamma_{\text{QCD+QED}_\text{II}}$
η_c	$\lambda_1 = 0, \lambda_2 = 1$	$20.34^{+10.37}_{-7.90}$	$18.91^{+10.05}_{-7.59}$	$27.96^{+3.16}_{-5.41}$	$28.27^{+3.44}_{-5.70}$
χ_{c0}	$\lambda_1 = 0, \lambda_2 = 1$	$1.45^{+1.07}_{-0.74}$	$1.49^{+1.08}_{-0.76}$	$1.58^{+0.01}_{-0.19}$	$1.57^{+0.01}_{-0.19}$
χ_{c1}	$\lambda_1 = 1, \lambda_2 = 1$	$0.28^{+0.12}_{-0.09}$	$0.25^{+0.11}_{-0.09}$	$0.34^{+0.03}_{-0.05}$	$0.34^{+0.03}_{-0.06}$
	$\lambda_1 = 0, \lambda_2 = 1$	$3.63^{+1.65}_{-1.29}$	$3.28^{+1.57}_{-1.22}$	$3.47^{+0.01}_{-0.30}$	$3.54^{+0.03}_{-0.37}$
χ_{c2}	$\lambda_1 = 2, \lambda_2 = 1$	$0.23^{+0.15}_{-0.10}$	$0.23^{+0.14}_{-0.10}$	$0.13^{+0.01}_{-0.003}$	$0.13^{+0.01}_{-0.001}$
	$\lambda_1 = 1, \lambda_2 = 1$	$0.59^{+0.37}_{-0.27}$	$0.58^{+0.37}_{-0.27}$	$0.35^{+0.02}_{-0.06}$	$0.35^{+0.02}_{-0.07}$
	$\lambda_1 = 0, \lambda_2 = 1$	$1.53^{+0.96}_{+0.69}$	$1.50^{+0.96}_{-0.69}$	$0.95^{+0.06}_{-0.23}$	$0.96^{+0.07}_{-0.25}$

the experimental measurement, even the perturbative expansion is of poor convergence.

Finally, for the sake of completeness, we present the NRQCD predictions for the channels involving radially excited heavy quarkonia in table 6, which may provide useful help for experimentalists.

Table 6. NRQCD predictions on the branching fraction of a vector bottomonium radiative decay into a charmonium. We choose $m_c = 1.483 \text{ GeV}$, $m_b = 4.580 \text{ GeV}$ and evaluate the LDMEs through the BT potential model. The masses of the quarkonia are taken from PDG [59]. The second row represents the branching fractions up to NLO in α_s , where the uncertainties originate from μ_R -dependence and $\Gamma_{\Upsilon(nS)}$. We display the experimental data from Belle [4] in the third row.

Channels	$\text{Br}(\times 10^{-5})$	Belle-2019 [4]
$\Upsilon \rightarrow \eta_c + \gamma$	$10.47^{+1.45}_{-2.28}$	< 2.9
$\Upsilon(2S) \rightarrow \eta_c + \gamma$	$8.74^{+1.53}_{-2.32}$	—
$\Upsilon(3S) \rightarrow \eta_c + \gamma$	$10.45^{+1.90}_{-2.87}$	—
$\Upsilon \rightarrow \eta_c(2S) + \gamma$	$6.84^{+0.94}_{-1.49}$	< 40
$\Upsilon \rightarrow \chi_{c0} + \gamma$	$0.58^{+0.01}_{-0.08}$	< 6.6
$\Upsilon \rightarrow \chi_{c1} + \gamma$	$1.44^{+0.04}_{-0.14}$	$4.7^{+2.4+0.4}_{-1.8-0.5}$
$\Upsilon \rightarrow \chi_{c2} + \gamma$	$0.53^{+0.05}_{-0.11}$	< 3.3
$\Upsilon(2S) \rightarrow \chi_{c0} + \gamma$	$0.49^{+0.03}_{-0.04}$	—
$\Upsilon(2S) \rightarrow \chi_{c1} + \gamma$	$1.19^{+0.09}_{-0.21}$	—
$\Upsilon(2S) \rightarrow \chi_{c2} + \gamma$	$0.45^{+0.05}_{-0.12}$	—
$\Upsilon(3S) \rightarrow \chi_{c0} + \gamma$	$0.60^{+0.04}_{-0.11}$	—
$\Upsilon(3S) \rightarrow \chi_{c1} + \gamma$	$1.41^{+0.10}_{-0.25}$	—
$\Upsilon(3S) \rightarrow \chi_{c2} + \gamma$	$0.55^{+0.06}_{-0.17}$	—

8 Summary

In this work, we compute the NLO QCD corrections to the radiative decay $\Upsilon \rightarrow \eta_c(\chi_{cJ}) + \gamma$ by applying the NRQCD factorization formalism. We choose two benchmark values of the masses of charm and bottom quarks: $m_c = 1.483$ GeV and $m_b = 4.580$ GeV, which corresponds to the one-loop heavy quark pole masses, and $m_c = 1.68$ GeV and $m_b = 4.78$ GeV, which corresponds to the two-loop heavy quark pole masses. We include both the QED and the QCD Feynman diagrams, the amplitudes of which are calculated up to NLO in α_s . The helicity amplitudes and the helicity decay widths are obtained. It is the first computation for the processes involving both bottomonium and charmonium at two-loop accuracy. By utilizing the Cheng-Wu theorem, we can convert most of the complex-valued MIs into real-valued MIs, which makes the numerical integration much efficient. In addition, we make use of two different schemes to deal with the QED contribution, and find a good agreement.

Our results indicate that the decay widths are dominated by the QCD contribution for χ_{c0} and χ_{c2} production, while the QED contribution is comparable to the QCD contribution for η_c and χ_{c1} production. We notice that the $\mathcal{O}(\alpha_s)$ corrections are moderate for η_c and χ_{c2} production, and are quite marginal for χ_{c0} and χ_{c1} production. It is interesting to note that the NLO corrections considerably reduce the renormalization scale dependence in the branching fractions of χ_{cJ} production, which may indicate a decent convergence in perturbative expansion. With the NRQCD LDMEs evaluated through the BT potential model, we find the decay width of η_c production is one-order-of-magnitude larger than those of χ_{cJ} production, which may provide a good opportunity to search for $\Upsilon \rightarrow \eta_c + \gamma$ in experiment. In addition, the decay width of χ_{c1} is several times larger than those of $\chi_{c0,2}$. Finally, we find the NRQCD prediction on the branching ratio of $\Upsilon \rightarrow \chi_{c1} + \gamma$ is only half of the lower bound of the experimental data measured by Belle. Moreover, there exists serious contradiction between theory and experiment for $\Upsilon \rightarrow \eta_c + \gamma$. The discrepancies between theory and experiment deserve further research efforts.

Acknowledgments

The work of Y.-D. Z. and W.-L. S. is supported by the National Natural Science Foundation of China under Grants No. 11975187 and the Natural Science Foundation of ChongQing under Grant No. cstc2019jcyj-msxmX0479. The work of F. F. is supported by the National Natural Science Foundation of China under Grant No. 11875318, No. 11505285, and by the Yue Qi Young Scholar Project in CUMTB. The work of H.-F. Zhang is supported by the National Natural Science Foundation of China under Grants No. 11965006.

Appendix

A Construction of various helicity projectors

In section 3, we have employed the helicity projectors to extract the corresponding helicity amplitudes of $\Upsilon \rightarrow H(\lambda_1) + \gamma(\lambda_2)$. In this appendix, we apply the similar approach used

in Ref. [67] to construct various helicity projectors $\mathcal{P}_{\lambda_1, \lambda_2}^{(H)}$.

For the sake of convenience, we introduce an auxiliary transverse metric tensor and two auxiliary longitudinal vectors,

$$g_{\perp}^{\mu\nu} = g^{\mu\nu} + \frac{P^\mu P^\nu}{|\mathbf{P}|^2} - \frac{Q \cdot P}{m_{\Upsilon}^2 |\mathbf{P}|^2} (P^\mu Q^\nu + Q^\mu P^\nu), \quad (\text{A.1a})$$

$$L_{\Upsilon}^\mu = \frac{1}{|\mathbf{P}|} \left(P^\mu - \frac{Q \cdot P}{m_{\Upsilon}^2} Q^\mu \right), \quad (\text{A.1b})$$

$$L_{\chi_{cJ}}^\mu = \frac{1}{|\mathbf{P}|} \left(\frac{P \cdot Q}{m_{\Upsilon} m_{\chi_{cJ}}} P^\mu - \frac{m_{\chi_{cJ}}}{m_{\Upsilon}} Q^\mu \right), \quad (\text{A.1c})$$

where P and Q denote the momenta of H and Υ mesons respectively, $m_{\chi_{cJ}}$ signifies the mass of χ_{cJ} . It is obvious the transverse metric tensor satisfies the properties

$$g_{\perp\mu\nu} P^\mu = g_{\perp\mu\nu} Q^\mu = 0, \quad (\text{A.2a})$$

$$g_{\perp\mu}^\mu = 2, \quad (\text{A.2b})$$

$$g_{\perp\mu\alpha} g_{\perp}^{\alpha\nu} = g_{\perp\mu\alpha} g^{\alpha\nu} = g_{\perp\mu}^\nu. \quad (\text{A.2c})$$

The longitudinal vectors satisfy $L_{\Upsilon}^\mu Q_\mu = L_{\chi_{cJ}}^\mu P_\mu = 0$.

The amplitude $\mathcal{A}^{(\eta_c)}$ of the process $\Upsilon \rightarrow \eta_c + \gamma$ can be parameterized as $\mathcal{A}^{(\eta_c)} = \mathcal{A}_{\mu\nu}^{(\eta_c)} \epsilon_{\Upsilon}^\mu \epsilon_{\gamma}^{*\nu}(\lambda_2)$, where ϵ_{Υ} and ϵ_{γ} denote the polarization vectors of Υ and γ , respectively. The unique helicity projector reads

$$\mathcal{P}_{0,1}^{(\eta_c)\mu\nu} = \frac{i}{2m_{\Upsilon}|\mathbf{P}|} \epsilon^{\mu\nu\rho\sigma} Q_{\rho} P_{\sigma}, \quad (\text{A.3})$$

which can be derived from the angular momentum conservation and parity conservation. Thus the helicity amplitude can be extracted by acting the helicity projector on the amputated amplitude $\mathcal{A}_{0,1}^{(\eta_c)} = \mathcal{P}_{0,1}^{(\eta_c)\mu\nu} \mathcal{A}_{\mu\nu}^{(\eta_c)}$.

Very similarly, the amplitude $\mathcal{A}^{(\chi_{c0})}$ of the process $\Upsilon \rightarrow \chi_{c0} + \gamma$ can be expressed as $\mathcal{A}^{(\chi_{c0})} = \mathcal{A}_{\mu\nu}^{(\chi_{c0})} \epsilon_{\Upsilon}^\mu \epsilon_{\gamma}^{*\nu}(\lambda_2)$. There is only one helicity projector corresponding to $\lambda_1 = 0$ and $\lambda_2 = 1$, which can be expressed as

$$\mathcal{P}_{0,1}^{(\chi_{c0})\mu\nu} = -\frac{1}{2} g_{\perp}^{\mu\nu}, \quad (\text{A.4})$$

which is quite different from the form of (A.3) because the parity of χ_{c0} is adverse to that of η_c . The helicity amplitude of χ_{c0} can be deduced by acting the helicity projector on the amputated amplitude $\mathcal{A}_{0,1}^{(\chi_{c0})} = \mathcal{P}_{0,1}^{(\chi_{c0})\mu\nu} \mathcal{A}_{\mu\nu}^{(\chi_{c0})}$.

By parameterizing the amplitude $\mathcal{A}^{(\chi_{c1})}$ of the process $\Upsilon \rightarrow \chi_{c1} + \gamma$ into $\mathcal{A}^{(\chi_{c1})} = \mathcal{A}_{\mu\nu\alpha}^{(\chi_{c1})} \epsilon_{\Upsilon}^\mu \epsilon_{\gamma}^{*\nu}(\lambda_2) \epsilon_{\chi_{c1}}^{*\alpha}(\lambda_1)$, we can deduce the two independent helicity projectors for χ_{c1}

$$\mathcal{P}_{1,1}^{(\chi_{c1})\mu\nu\alpha} = \frac{-1}{2m_{\Upsilon}|\mathbf{P}|} L_{\Upsilon}^\mu \epsilon^{\nu\alpha\rho\sigma} Q_{\rho} P_{\sigma}, \quad (\text{A.5a})$$

$$\mathcal{P}_{0,1}^{(\chi_{c1})\mu\nu\alpha} = \frac{1}{2m_{\Upsilon}|\mathbf{P}|} L_{\chi_{c1}}^\alpha \epsilon^{\mu\nu\rho\sigma} Q_{\rho} P_{\sigma}. \quad (\text{A.5b})$$

The corresponding two helicity amplitudes of χ_{c1} can be readily obtained by acting the helicity projectors on the amputated amplitude: $\mathcal{A}_{0,1}^{(\chi_{c1})} = \mathcal{P}_{0,1}^{(\chi_{c1})\mu\nu\alpha} \mathcal{A}_{\mu\nu\alpha}^{(\chi_{c1})}$ and $\mathcal{A}_{1,1}^{(\chi_{c1})} = \mathcal{P}_{1,1}^{(\chi_{c1})\mu\nu\alpha} \mathcal{A}_{\mu\nu\alpha}^{(\chi_{c1})}$.

Finally, if we express the amplitude $\mathcal{A}^{(\chi_{c2})}$ of the process $\Upsilon \rightarrow \chi_{c2} + \gamma$ into $\mathcal{A}_{\mu\nu\alpha\beta}^{(\chi_{c2})} \epsilon_{\Upsilon}^{\mu} \epsilon_{\gamma}^{*\nu}(\lambda_2) \epsilon_{\chi_{c2}}^{*\alpha\beta}(\lambda_1)$, the three independent helicity projectors for χ_{c2} can be deduced

$$\mathcal{P}_{2,1}^{(\chi_{c2})\mu\nu\alpha\beta} = \frac{1}{4} \left(g_{\perp}^{\mu\nu} g_{\perp}^{\alpha\beta} - g_{\perp}^{\mu\alpha} g_{\perp}^{\nu\beta} - g_{\perp}^{\mu\beta} g_{\perp}^{\nu\alpha} \right), \quad (\text{A.6a})$$

$$\mathcal{P}_{1,1}^{(\chi_{c2})\mu\nu\alpha\beta} = \frac{-1}{2\sqrt{2}} L_{\Upsilon}^{\mu} \left(g_{\perp}^{\nu\alpha} L_{\chi_{c2}}^{\beta} + g_{\perp}^{\nu\beta} L_{\chi_{c2}}^{\alpha} \right), \quad (\text{A.6b})$$

$$\mathcal{P}_{0,1}^{(\chi_{c2})\mu\nu\alpha\beta} = \frac{-1}{2\sqrt{6}} g_{\perp}^{\mu\nu} \left(g_{\perp}^{\alpha\beta} + 2 L_{\chi_{c2}}^{\alpha} L_{\chi_{c2}}^{\beta} \right). \quad (\text{A.6c})$$

The corresponding helicity amplitudes for χ_{c2} can be readily obtained by acting the helicity projectors on the amputated amplitude: $\mathcal{A}_{2,1}^{(\chi_{c2})} = \mathcal{P}_{2,1}^{(\chi_{c2})\mu\nu\alpha\beta} \mathcal{A}_{\mu\nu\alpha\beta}^{(\chi_{c2})}$, $\mathcal{A}_{1,1}^{(\chi_{c2})} = \mathcal{P}_{1,1}^{(\chi_{c2})\mu\nu\alpha\beta} \mathcal{A}_{\mu\nu\alpha\beta}^{(\chi_{c2})}$ and $\mathcal{A}_{0,1}^{(\chi_{c2})} = \mathcal{P}_{0,1}^{(\chi_{c2})\mu\nu\alpha\beta} \mathcal{A}_{\mu\nu\alpha\beta}^{(\chi_{c2})}$.

Since we do not consider the relativistic corrections in this work, it is eligible to make the approximations $m_{\Upsilon} \approx 2m_b$, $m_{\eta_c} \approx 2m_c$, and $m_{\chi_{cJ}} \approx 2m_c$ in the helicity projectors.

B Applying the Cheng-Wu theorem to deal with loop integrals

The description about Cheng-Wu theorem can be found in Refs. [53–55, 68]. In Ref. [69], the authors have successfully gotten rid of the nontrivial Heaviside step function through Cheng-Wu theorem. In Ref. [70], one of our authors has applied the Cheng-Wu theorem to evaluate some special integrals. In this appendix, we further extend the application of Cheng-Wu theorem in multi-loop integration.

The function \mathcal{F} is projective, if it satisfies

$$\mathcal{F}(\lambda x_1, \dots, \lambda x_n) = \lambda^{-n} \mathcal{F}(x_1, \dots, x_n). \quad (\text{B.1})$$

The Cheng-Wu theorem indicates that the integral \mathcal{I}

$$\mathcal{I} = \int_0^{\infty} dx_1 \cdots \int_0^{\infty} dx_n \mathcal{F}(x_1, \dots, x_n) \delta\left(1 - \sum_{i=1}^n a_i x_i\right) \quad (\text{B.2})$$

does not depend on the set $\{a_i\}$, when all variables in $\{x_i\}$ are nonnegative and at least one a_i is positive, i.e., $\forall i, a_i \geq 0$ and $\exists k, a_k > 0$. The theorem might be employed to eliminate the negative terms in \mathcal{F} .

After the alpha-representation, the Feynman multi-loop integrals can be generally transferred into the following form

$$\mathcal{I} = \int_0^{\infty} d\mathbf{x} \delta\left(1 - \sum_{i=1}^n x_i\right) U(\mathbf{x})^a F(\mathbf{x})^b, \quad (\text{B.3})$$

where \mathbf{x} denotes the set $\{x_i\}$, and the exponents a and b are linear in ϵ with the dimension of the spacetime $d = 4 - 2\epsilon$. It can be proved that eq. (B.3) conforms to the form of (B.2).

The U term and F term are the polynomials of \mathbf{x} . In the physical region, the F term may contain negative terms. In the following, we describe the strategy to eliminate the negative terms in F by employing the Cheng-Wu theorem (B.2). Since the U term is irrelevant to the discussion, we will suppress the U term in the remainder of this appendix.

We introduce how to eliminate the negative terms in F through three specific cases.

Case 1: If F can be expressed into $F = \mathcal{P}(\hat{\mathbf{x}}_k) - x_k \mathcal{Q}(\hat{\mathbf{x}}_k) - i\varepsilon$, where $\hat{\mathbf{x}}_k$ denotes the set $\{x_i\}$ with the variable x_k removed, and \mathcal{P} and \mathcal{Q} are positive polynomials of $\hat{\mathbf{x}}_k$. We are able to pull x_k outside the δ -function through setting $a_k = 0$ in eq. (B.2), and then rescale x_k through

$$x_k = \frac{\mathcal{P}(\hat{\mathbf{x}}_k)}{\mathcal{Q}(\hat{\mathbf{x}}_k)} \frac{y_k}{x_j}, \quad (\text{B.4})$$

where we call x_j the label variable which should be different from x_k . After renaming y_k with x_k and putting x_k back inside δ -function by the Cheng-Wu theorem, we finally obtain

$$\mathcal{I} = \int_0^\infty d\mathbf{x} \delta(1 - \sum_{i=1}^n x_i) \frac{\mathcal{P}^{b+1}}{x_j^{b+1} \mathcal{Q}} (x_j - x_k - i\varepsilon)^b, \quad (\text{B.5})$$

where we have suppressed the arguments of \mathcal{P} and \mathcal{Q} for simplification. After the transformation, the new F term turns to be $x_j - x_k - i\varepsilon$. Splitting the integration domain into two parts $x_j \leq x_k$ and $x_j \geq x_k$ through the transformations

$$x_k = x_j + x_k \quad (\text{B.6})$$

and

$$x_j = x_j + x_k, \quad (\text{B.7})$$

we can convert the F term either into a fully positive polynomial or into a fully negative polynomial, where the F term can be further turned to be positive by an overall constant phase factor for the latter case.

Case 2: If F can be expressed into $F = \mathcal{P}(\hat{\mathbf{x}}_{kl}) - x_k \mathcal{Q}_k(\hat{\mathbf{x}}_{kl}) - x_l \mathcal{Q}_l(\hat{\mathbf{x}}_l) - i\varepsilon$, where $\hat{\mathbf{x}}_{kl}$ denotes the set $\{x_i\}$ with both x_k and x_l removed, and \mathcal{P} , \mathcal{Q}_k and \mathcal{Q}_l are positive polynomials. We can first pull x_k and x_l outside the δ -function, and then rescale the two variables

$$x_l = \frac{\mathcal{P}(\hat{\mathbf{x}}_{kl})}{\mathcal{Q}_l(\hat{\mathbf{x}}_l)} \frac{y_l}{x_j}, \quad x_k = \frac{\mathcal{P}(\hat{\mathbf{x}}_{kl})}{\mathcal{Q}_k(\hat{\mathbf{x}}_{kl})} \frac{y_k}{x_j}, \quad (\text{B.8})$$

where we call x_j the label variable which should be different from x_k and x_l . After renaming y_k and y_l with x_k and x_l respectively, and putting x_k and x_l back inside the δ -function by the Cheng-Wu theorem, we then obtain

$$\mathcal{I} = \int_0^\infty d\mathbf{x} \delta(1 - \sum_i x_i) \frac{\mathcal{P}(\hat{\mathbf{x}}_k)^{b+2}}{x_j^{b+2} \mathcal{Q}_l(\hat{\mathbf{x}}_l) \mathcal{Q}_k(\hat{\mathbf{x}}_{kl})} (x_j - x_k - x_l - i\varepsilon)^b. \quad (\text{B.9})$$

Now the new F term becomes $x_j - x_k - x_l - i\varepsilon$. Once again, by pulling x_j outside the δ -function, rescaling x_j according to

$$x_j = (x_k + x_l) \frac{y_j}{x_k}, \quad (\text{B.10})$$

renaming y_j with x_j , and putting x_j back inside the δ -function, we finally arrive at

$$\mathcal{I} = \int_0^\infty d\mathbf{x} \delta(1 - \sum_i x_i) \frac{\mathcal{P}^{b+2}}{x_j^{b+2}} \frac{x_k}{x_k + x_l} \frac{1}{\mathcal{Q}_l} \frac{1}{\mathcal{Q}_k} (x_j - x_k - i\epsilon)^b. \quad (\text{B.11})$$

We can further divide the integration domain into two parts $x_j \leq x_k$ and $x_j \geq x_k$ through the transformations

$$x_k = x_j + x_k, \quad (\text{B.12})$$

and

$$x_j = x_j + x_k. \quad (\text{B.13})$$

We end up with either a positive F polynomial or a fully negative F polynomial which can be turned to be positive by an overall constant phase factor.

Case 3: If F can be expressed into $F = \mathcal{P}(\hat{\mathbf{x}}_{kl}) - x_k[\mathcal{Q}_k(\hat{\mathbf{x}}_{kl}) - x_l\mathcal{Q}_l(\hat{\mathbf{x}}_{kl})] - i\epsilon$, where \mathcal{P} , \mathcal{Q}_k and \mathcal{Q}_l are positive polynomials. We first pull x_l outside the δ -function, and then rescale x_l by

$$x_l = \frac{\mathcal{Q}_k(\hat{\mathbf{x}}_{kl})}{\mathcal{Q}_l(\hat{\mathbf{x}}_{kl})} \frac{y_l}{x_j}, \quad (\text{B.14})$$

where x_j is called label variable which should be different from x_k and x_l . By repeating the same procedure, we are able to put x_l back inside δ -function. After the transformation, the F term now becomes $\mathcal{P}(\hat{\mathbf{x}}_{kl}) - x_k \frac{\mathcal{Q}_k(\hat{\mathbf{x}}_{kl})}{x_j} (x_j - x_l) - i\epsilon$. The integration domain can be divided into two parts: $x_j \leq x_l$ through the transformation

$$x_l = x_j + x_l, \quad (\text{B.15})$$

and $x_j \geq x_l$ through

$$x_j = x_j + x_l. \quad (\text{B.16})$$

In the domain $x_j \leq x_l$, the F term is obvious positive. For $x_j \geq x_l$, the F term is of the same form as that in *Case 1*, thus we can repeat the procedure in *Case 1* to transfer the F term positive.

Through the Cheng-Wu theorem, we can convert most of the complex-valued MIs encountered in this work into the real-valued MIs, which makes the numerical integration much efficient.

References

- [1] C. P. Shen *et al.* [Belle], Phys. Rev. D **82** (2010), 051504 doi:10.1103/PhysRevD.82.051504 [arXiv:1008.1774 [hep-ex]].
- [2] X. L. Wang *et al.* [Belle], Phys. Rev. D **84** (2011), 071107 doi:10.1103/PhysRevD.84.071107 [arXiv:1108.4514 [hep-ex]].
- [3] C. P. Shen [Belle], [arXiv:1208.0900 [hep-ex]].
- [4] P. Katrenko *et al.* [Belle], Phys. Rev. Lett. **124** (2020) no.12, 122001 doi:10.1103/PhysRevLett.124.122001 [arXiv:1910.10915 [hep-ex]].

- [5] G. T. Bodwin, E. Braaten and G. P. Lepage, Phys. Rev. D **51** (1995), 1125-1171 [erratum: Phys. Rev. D **55** (1997), 5853] doi:10.1103/PhysRevD.55.5853 [arXiv:hep-ph/9407339 [hep-ph]].
- [6] Y. J. Gao, Y. J. Zhang and K. T. Chao, [arXiv:hep-ph/0701009 [hep-ph]].
- [7] D. D. Shen, C. Y. Lu, P. Sun and R. Zhu, [arXiv:2011.03942 [hep-ph]].
- [8] G. Hao, Y. Jia, C. F. Qiao and P. Sun, JHEP **02** (2007), 057 doi:10.1088/1126-6708/2007/02/057 [arXiv:hep-ph/0612173 [hep-ph]].
- [9] A. Czarnecki and K. Melnikov, Phys. Rev. Lett. **80** (1998), 2531-2534 doi:10.1103/PhysRevLett.80.2531 [arXiv:hep-ph/9712222 [hep-ph]].
- [10] M. Beneke, A. Signer and V. A. Smirnov, Phys. Rev. Lett. **80** (1998), 2535-2538 doi:10.1103/PhysRevLett.80.2535 [arXiv:hep-ph/9712302 [hep-ph]].
- [11] P. Marquard, J. H. Piclum, D. Seidel and M. Steinhauser, Phys. Rev. D **89** (2014) no.3, 034027 doi:10.1103/PhysRevD.89.034027 [arXiv:1401.3004 [hep-ph]].
- [12] M. Beneke, Y. Kiyo, P. Marquard, A. Penin, J. Piclum, D. Seidel and M. Steinhauser, Phys. Rev. Lett. **112** (2014) no.15, 151801 doi:10.1103/PhysRevLett.112.151801 [arXiv:1401.3005 [hep-ph]].
- [13] A. Czarnecki and K. Melnikov, Phys. Lett. B **519** (2001), 212-218 doi:10.1016/S0370-2693(01)01129-7 [arXiv:hep-ph/0109054 [hep-ph]].
- [14] F. Feng, Y. Jia and W. L. Sang, Phys. Rev. Lett. **115** (2015) no.22, 222001 doi:10.1103/PhysRevLett.115.222001 [arXiv:1505.02665 [hep-ph]].
- [15] A. I. Onishchenko and O. L. Veretin, Eur. Phys. J. C **50** (2007), 801-808 doi:10.1140/epjc/s10052-007-0255-1 [arXiv:hep-ph/0302132 [hep-ph]].
- [16] L. B. Chen and C. F. Qiao, Phys. Lett. B **748** (2015), 443-450 doi:10.1016/j.physletb.2015.07.043 [arXiv:1503.05122 [hep-ph]].
- [17] W. L. Sang, F. Feng, Y. Jia and S. R. Liang, Phys. Rev. D **94** (2016) no.11, 111501 doi:10.1103/PhysRevD.94.111501 [arXiv:1511.06288 [hep-ph]].
- [18] F. Feng, Y. Jia and W. L. Sang, Phys. Rev. Lett. **119** (2017) no.25, 252001 doi:10.1103/PhysRevLett.119.252001 [arXiv:1707.05758 [hep-ph]].
- [19] S. Q. Wang, X. G. Wu, W. L. Sang and S. J. Brodsky, Phys. Rev. D **97** (2018) no.9, 094034 doi:10.1103/PhysRevD.97.094034 [arXiv:1804.06106 [hep-ph]].
- [20] F. Feng, Y. Jia and W. L. Sang, [arXiv:1901.08447 [hep-ph]].
- [21] L. B. Chen, Y. Liang and C. F. Qiao, JHEP **01** (2018), 091 doi:10.1007/JHEP01(2018)091 [arXiv:1710.07865 [hep-ph]].
- [22] W. L. Sang, F. Feng and Y. Jia, JHEP **10** (2020), 098 doi:10.1007/JHEP10(2020)098 [arXiv:2008.04898 [hep-ph]].
- [23] H. M. Yu, W. L. Sang, X. D. Huang, J. Zeng, X. G. Wu and S. J. Brodsky, [arXiv:2007.14553 [hep-ph]].
- [24] L. Yang, W. L. Sang, H. F. Zhang, Y. D. Zhang and M. Z. Zhou, Phys. Rev. D **103** (2021) no.3, 034018 doi:10.1103/PhysRevD.103.034018 [arXiv:2010.14364 [hep-ph]].
- [25] H. E. Haber, [arXiv:hep-ph/9405376 [hep-ph]].

- [26] V. L. Chernyak and A. R. Zhitnitsky, Sov. J. Nucl. Phys. **31** (1980), 544-552
- [27] S. J. Brodsky and G. P. Lepage, Phys. Rev. D **24** (1981), 2848
doi:10.1103/PhysRevD.24.2848
- [28] A. Petrelli, M. Cacciari, M. Greco, F. Maltoni and M. L. Mangano, Nucl. Phys. B **514** (1998), 245-309 doi:10.1016/S0550-3213(97)00801-8 [arXiv:hep-ph/9707223 [hep-ph]].
- [29] G. T. Bodwin and A. Petrelli, Phys. Rev. D **66** (2002), 094011 [erratum: Phys. Rev. D **87** (2013) no.3, 039902] doi:10.1103/PhysRevD.66.094011 [arXiv:hep-ph/0205210 [hep-ph]].
- [30] D. Binosi, J. Collins, C. Kaufhold and L. Theussl, Comput. Phys. Commun. **180** (2009), 1709-1715 doi:10.1016/j.cpc.2009.02.020 [arXiv:0811.4113 [hep-ph]].
- [31] T. Hahn, Comput. Phys. Commun. **140** (2001), 418-431 doi:10.1016/S0010-4655(01)00290-9 [arXiv:hep-ph/0012260 [hep-ph]].
- [32] R. Mertig, M. Bohm and A. Denner, Comput. Phys. Commun. **64** (1991), 345-359
doi:10.1016/0010-4655(91)90130-D
- [33] V. Shtabovenko, R. Mertig and F. Orellana, Comput. Phys. Commun. **207** (2016), 432-444
doi:10.1016/j.cpc.2016.06.008 [arXiv:1601.01167 [hep-ph]].
- [34] F. Feng and R. Mertig, [arXiv:1212.3522 [hep-ph]].
- [35] M. Beneke and V. A. Smirnov, Nucl. Phys. B **522** (1998), 321-344
doi:10.1016/S0550-3213(98)00138-2 [arXiv:hep-ph/9711391 [hep-ph]].
- [36] F. Feng, Comput. Phys. Commun. **183** (2012), 2158-2164 doi:10.1016/j.cpc.2012.03.025
[arXiv:1204.2314 [hep-ph]].
- [37] A. V. Smirnov, Comput. Phys. Commun. **189** (2015), 182-191 doi:10.1016/j.cpc.2014.11.024
[arXiv:1408.2372 [hep-ph]].
- [38] H. H. Patel, Comput. Phys. Commun. **197** (2015), 276-290 doi:10.1016/j.cpc.2015.08.017
[arXiv:1503.01469 [hep-ph]].
- [39] A. V. Smirnov, Comput. Phys. Commun. **185** (2014), 2090-2100
doi:10.1016/j.cpc.2014.03.015 [arXiv:1312.3186 [hep-ph]].
- [40] T. Binoth and G. Heinrich, Nucl. Phys. B **585** (2000), 741-759
doi:10.1016/S0550-3213(00)00429-6 [arXiv:hep-ph/0004013 [hep-ph]].
- [41] T. Binoth and G. Heinrich, Nucl. Phys. B **680** (2004), 375-388
doi:10.1016/j.nuclphysb.2003.12.023 [arXiv:hep-ph/0305234 [hep-ph]].
- [42] T. Binoth and G. Heinrich, Nucl. Phys. B **693** (2004), 134-148
doi:10.1016/j.nuclphysb.2004.06.005 [arXiv:hep-ph/0402265 [hep-ph]].
- [43] G. Heinrich, Int. J. Mod. Phys. A **23** (2008), 1457-1486 doi:10.1142/S0217751X08040263
[arXiv:0803.4177 [hep-ph]].
- [44] C. Bogner and S. Weinzierl, Comput. Phys. Commun. **178** (2008), 596-610
doi:10.1016/j.cpc.2007.11.012 [arXiv:0709.4092 [hep-ph]].
- [45] C. Bogner and S. Weinzierl, Nucl. Phys. B Proc. Suppl. **183** (2008), 256-261
doi:10.1016/j.nuclphysbps.2008.09.113 [arXiv:0806.4307 [hep-ph]].
- [46] R. Cools and A. Haegemans, ACM Trans. Math. Softw. **29** (2003), no. 3 287 C296.

- [47] S. Borowka and G. Heinrich, PoS **LL2012** (2012), 037 doi:10.22323/1.151.0037 [arXiv:1209.6345 [hep-ph]].
- [48] <https://github.com/stevengj/cubature>, HCubature web site
- [49] D. J. Broadhurst, N. Gray and K. Schilcher, Z. Phys. C **52** (1991), 111-122 doi:10.1007/BF01412333
- [50] K. Melnikov and T. van Ritbergen, Nucl. Phys. B **591** (2000), 515-546 doi:10.1016/S0550-3213(00)00526-5 [arXiv:hep-ph/0005131 [hep-ph]].
- [51] P. Bärnreuther, M. Czakon and P. Fiedler, JHEP **02** (2014), 078 doi:10.1007/JHEP02(2014)078 [arXiv:1312.6279 [hep-ph]].
- [52] S. Borowka, G. Heinrich, S. Jahn, S. P. Jones, M. Kerner, J. Schlenk and T. Zirke, Comput. Phys. Commun. **222** (2018), 313-326 doi:10.1016/j.cpc.2017.09.015 [arXiv:1703.09692 [hep-ph]].
- [53] H. Cheng and T. T. Wu, *Expanding Protons: Scattering at High Energies* (MIT Press, Cambridge, MA, 1987).
- [54] V. A. Smirnov, *Evaluating Feynman integrals* (Springer Tracts Mod. Phys. **211**, 2004), <http://www.springer.com/physics/particle+and+nuclear+physics/book/978-3-540-23933-8>.
- [55] K. S. Bjoerkevold, P. Osland and G. Faeldt, Nucl. Phys. B **386** (1992), 303-342 doi:10.1016/0550-3213(92)90569-W
- [56] G. T. Bodwin, H. S. Chung, J. H. Ee and J. Lee, Phys. Rev. D **97** (2018) no.1, 016009 doi:10.1103/PhysRevD.97.016009 [arXiv:1709.09320 [hep-ph]].
- [57] W. L. Sang and Y. Q. Chen, Phys. Rev. D **81** (2010), 034028 doi:10.1103/PhysRevD.81.034028 [arXiv:0910.4071 [hep-ph]].
- [58] K. G. Chetyrkin, J. H. Kuhn and M. Steinhauser, Comput. Phys. Commun. **133** (2000), 43-65 doi:10.1016/S0010-4655(00)00155-7 [arXiv:hep-ph/0004189 [hep-ph]].
- [59] P. A. Zyla *et al.* [Particle Data Group], PTEP **2020** (2020) no.8, 083C01 doi:10.1093/ptep/ptaa104
- [60] G. T. Bodwin, H. S. Chung, D. Kang, J. Lee and C. Yu, Phys. Rev. D **77** (2008), 094017 doi:10.1103/PhysRevD.77.094017 [arXiv:0710.0994 [hep-ph]].
- [61] H. K. Guo, Y. Q. Ma and K. T. Chao, Phys. Rev. D **83** (2011), 114038 doi:10.1103/PhysRevD.83.114038 [arXiv:1104.3138 [hep-ph]].
- [62] G. T. Bodwin, S. Kim and D. K. Sinclair, Nucl. Phys. B Proc. Suppl. **34** (1994), 434-436 doi:10.1016/0920-5632(94)90410-3
- [63] G. T. Bodwin, D. K. Sinclair and S. Kim, Phys. Rev. Lett. **77** (1996), 2376-2379 doi:10.1103/PhysRevLett.77.2376 [arXiv:hep-lat/9605023 [hep-lat]].
- [64] G. T. Bodwin, D. K. Sinclair and S. Kim, Phys. Rev. D **65** (2002), 054504 doi:10.1103/PhysRevD.65.054504 [arXiv:hep-lat/0107011 [hep-lat]].
- [65] H. S. Chung, JHEP **12** (2020), 065 doi:10.1007/JHEP12(2020)065 [arXiv:2007.01737 [hep-ph]].
- [66] E. J. Eichten and C. Quigg, Phys. Rev. D **52** (1995), 1726-1728 doi:10.1103/PhysRevD.52.1726 [arXiv:hep-ph/9503356 [hep-ph]].

- [67] J. Xu, H. R. Dong, F. Feng, Y. J. Gao and Y. Jia, Phys. Rev. D **87** (2013) no.9, 094004
doi:10.1103/PhysRevD.87.094004 [arXiv:1212.3591 [hep-ph]].
- [68] B. Jantzen, A. V. Smirnov and V. A. Smirnov, Eur. Phys. J. C **72** (2012), 2139
doi:10.1140/epjc/s10052-012-2139-2 [arXiv:1206.0546 [hep-ph]].
- [69] W. L. Sang, F. Feng and Y. Jia, Phys. Rev. D **102** (2020) no.9, 094021
doi:10.1103/PhysRevD.102.094021 [arXiv:2010.11896 [hep-ph]].
- [70] F. Feng, Y. F. Xie, Q. C. Zhou and S. R. Tang, Comput. Phys. Commun. **265** (2021), 107982
doi:10.1016/j.cpc.2021.107982 [arXiv:2103.08507 [hep-ph]]. Copy to Clipboard Download